

Polarization-sensitive near-field investigation of photonic crystal microcavities

Silvia Vignolini,^{1,a)} Francesca Intonti,² Francesco Riboli,¹ Diederik S. Wiersma,¹ Laurent Balet,³ Lianhe H. Li,³ Marco Francardi,⁴ Annamaria Gerardino,⁴ Andrea Fiore,⁵ and Massimo Gurioli²

¹*LENS and INFN-BEC, Via Nello Carrara 1, 50019 Sesto Fiorentino Italy*

²*CNISM, Unità di Ricerca di Firenze and Department of Physics, Via Sansone 1, 50019 Sesto Fiorentino, Italy*

³*EPFL Institute of Photonics and Quantum Electronics, Station 3, CH-1015 Lausanne, Switzerland*

⁴*Institute of Photonics and Nanotechnology, CNR, via del Cineto Romano 42, 00156 Roma, Italy*

⁵*COBRA Research Institute, Eindhoven University of Technology, 5600 MB Eindhoven, The Netherlands*

(Received 28 January 2009; accepted 21 March 2009; published online 20 April 2009)

We report on polarization sensitive imaging of two-dimensional photonic crystal microcavity modes. By using a near-field scanning optical microscope with a polarization sensitive setup, it is possible to selectively map, with a resolution beyond the diffraction limit, each electric field component in the plane of the sample. In addition, the simultaneous analysis of photoluminescence maps in different polarization channels allowed us to obtain important insight on near-field microscopy detection mechanism. Finite difference time domain simulations confirm the experimental results. © 2009 American Institute of Physics. [DOI: 10.1063/1.3118578]

In the past few years, photonic crystal microcavities (PC-MCs) have been intensively studied and improved both for their potential applications in the field of optoelectronics as well as for their fundamental physical properties.^{1,2} The geometry of the PC-MCs defines both the spatial distribution and the polarization properties of the optical modes, and the possibility to control and combine these two degrees of freedom is of the utmost interest for the realization of several applications, such as PC based lasers³ or photonic fibers.⁴

Up to now, the PC-MCs polarization properties have been studied mainly by far-field microscopy.³⁻⁷ In order to achieve a better spatial resolution, scanning near-field microscopy has already proved to be a powerful tool for addressing the optical modes of PC based devices.⁸⁻²⁰ Moreover, it was recently demonstrated that the spectral shift of the cavity modes induced by the local probe directly maps the electric field intensity, providing an additional imaging option with higher spatial resolution.¹⁵⁻¹⁸ However, even if particular configurations of near-field optical microscopes allow to control the polarization properties of light^{20,21} a direct correlation between the spatial map and the polarization of the electromagnetic modes of PC-MCs has not yet been obtained.

In this paper we demonstrate, by using a scanning near field microscope with polarization control, that it is possible to completely retrace the vectorial maps of the electric field associated to the optical modes. By exploiting the advantage of the tip-induced spectral shift we are able to map the total electric field intensity associated to the mode. At the same time, the intensity maps of the photoluminescence (PL) signal of the mode, in the two orthogonal polarization channels, provide the imaging of the two electric field components in the plane of the PC-MC membrane.

The sample under consideration is a two dimensional PC-MC on a suspended membrane incorporating quantum

dots (QDs) acting as local light sources. The sample consists of a GaAs based heterostructure: three layers of high-density InAs QDs emitting at 1300 nm are grown by molecular beam epitaxy at the center of a 320-nm-thick GaAs membrane. The membrane is grown on top of a 1500-nm-thick Al_{0.7}Ga_{0.3}As sacrificial layer.²² The studied structure consists of a two-dimensional triangular lattice of air holes with lattice parameter $a=301$ nm and filling fraction $f=35\%$, where the cavity is formed by four missing holes organized in a diamondlike geometry. An in-plane scanning electron microscope image of the PC-MC is reported in Fig. 1(a), together with the (x, y, θ) reference system, to which we will refer for the polarization configurations; the direction $\theta=0^\circ$ ($\theta=90^\circ$) denotes the x (y) axis. A preliminary far-field characterization of the sample (via micro-PL at room temperature) is obtained using a 100 \times microscopy objective and a single-mode optical fiber with a 5 μm core diameter acting as confocal pinhole. The polarization-dependent spectrum of the cavity mode signal is measured by using a linear polarizer and by rotating a half-wave plate in front of the collection. Figure 1(b) shows the θ angular dependence of the PL peak intensity for the two main cavity modes, hereafter labeled M1 [black circles in Fig. 1(b)] and M2 [red squares in Fig. 1(b)], centered around 1263 and 1240.5 nm, respectively [see Fig. 1(c)]. The mode M1 is mainly polarized along the x direction (the ratio between opposite polarizations in the plane is 1:100), while the mode M2 is characterized by an elliptical polarization (the ratio between opposite polarizations in the plane is 1:2) along the y direction. The experimental spectral and polarization features of the two cavity peaks is well reproduced by calculations obtained by using a commercially available finite-difference time-domain (FDTD) solver package (Crystal Wave), as reported in Fig. 1(d), where the simulated emission spectra for the two in-plane components of the electric field are shown.

In order to map the spatial distribution of the electric field associated to these modes, we use a commercial scan-

^{a)}Electronic mail: vignolini@lens.unifi.it.

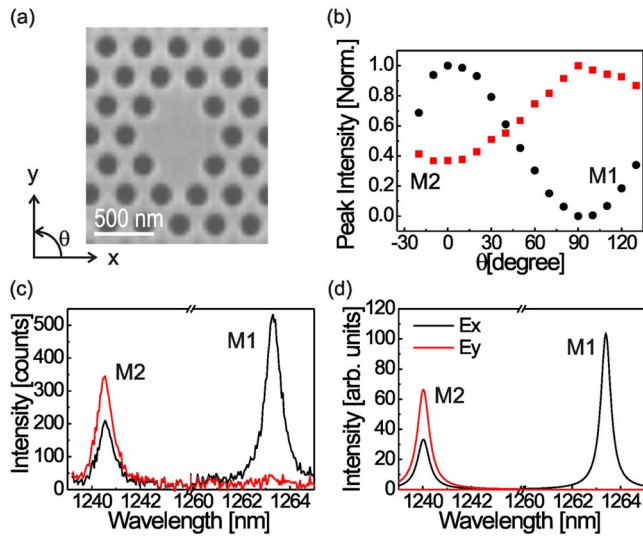


FIG. 1. (Color online) (a) Scanning electron microscope image of the investigated sample. In the figure we have drawn the (x, y, θ) reference system for describing the polarization configurations. (b) Polarization dependency of far-field emission (micro-PL) from the two main cavity peaks: M1 (black dots) and M2 (red squares). (c) Near-field spectra of the cavity main modes for the perpendicular x (black line) and y (red line) polarization configurations. (d) FDTD Calculation of the polarization dependency of the peaks. Note the break of the λ axis in (c) and (d).

ning near-field optical microscope (SNOM) [TwinSNOM, Omicron] in illumination/collection geometry. In this configuration, the sample is excited with light from a diode laser (780 nm) coupled into a chemically etched, uncoated near-field fiber probe,²³ that is raster scanned at a constant height on the sample surface. A portion of the PL signal of the embedded QDs is coupled to the same probe, passes through a linear polarizer, is dispersed by a spectrometer (resolution 0.1 nm), and finally it is detected by a cooled InGaAs array. All the data reported in this letter refer to room temperature. We control the polarization of the light in our SNOM experiment by using a non-polarization maintaining fiber and a polarization compensator acting on the fiber. Each photon, collected by the tip, changes its polarization state during the propagation along the fiber. This unknown polarization change is, however, identical for all the collected photons and therefore can be totally compensated. The polarization compensation is obtained using a system based on the Babinet–Soleil compensator that permit to apply a controlled pressure and rotation to the fiber. By changing the configuration of the polarization compensator and fixing the angle of the polarizer in front of the spectrometer, we can selectively collect only one polarization channel in the plane of the membrane. Moreover, since the selection of the polarization channel takes place at the end of the fiber, it does not play a role in the interaction between the near-field probe and the photonic structure.

A test of the polarization control in SNOM spectra is reported in Fig. 1(c), where the near-field spectra (averaged in a region of $2 \times 2 \mu\text{m}^2$) for two different polarization channels are provided. The red curve in Fig. 1(c) refers to the spectrum for the E_y polarization channel (where the signal of the mode M1 disappears) while the black line in Fig. 1(c) refers to the spectrum in the orthogonal E_x polarization channel. A pretty large extinction factor (1:100) is obtained in the SNOM spectra, denoting the sensitivity of our setup. Since the mode M1 is prevalently characterized by only one com-

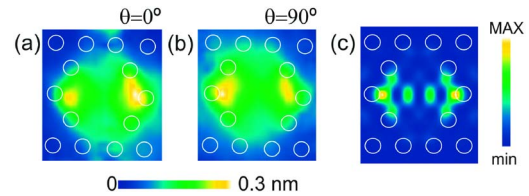


FIG. 2. (Color online) [(a) and (b)] Spectral shift maps in blue to white (black to white) colorscale associated to the mode M2 for the polarization configuration with $\theta=0^\circ$ and $\theta=90^\circ$, respectively (images size $1.55 \times 1.55 \mu\text{m}^2$). The two maps have the same intensity scale and they are smoothed to improve the quality of the images. (c) Calculated electric field distribution of the mode M2 at 30 nm above the photonic membrane. The calculations are performed using the nominal parameter of the structure with a refractive index of 3.48 and a spatial grid of 25 nm. The white circles superimposed on the images denote the topographic positions of the pores of the photonic structure.

ponent of the electric field, in the following we will focus the discussion on the results for the mode M2.

In order to obtain a high resolution image of the electric field intensity associated to the mode and to discuss the possible degenerate nature of M2, it is convenient to study the tip-induced spectral shift of the optical mode.^{15,16} In particular, we want to address the point whether the resonance M2 is composed by two orthogonal modes at the same wavelength or it is a single nondegenerate mode with both x and y components of the electric field. The tip-induced spectral shift depends on both the geometry of the tip and on the electric field intensity associated to the mode itself. By assuming that the tip has a circular geometry, we expect that its interaction does not depend on the electric field orientation. However, in the case of degenerate modes with different electric field spatial distribution and orthogonal polarization, a local perturbation acts differently for the two modes, possibly breaking the degeneracy.⁵ As a consequence, for such kind of modes, we expect to observe different spatial maps of the tip-induced spectral shift in the two orthogonal polarization channels. On the contrary, in the case of nondegenerate modes, the spectral shift maps are independent on the polarization configuration in the detection. Figure 2 shows (in a blue-to-white color scale) the results of the measured tip induced spectral shift for the mode M2 in two perpendicular polarization configurations (x and y , respectively), as compared with the theoretical calculation of the electric field intensity, Fig. 2(c). The comparison between experimental and simulated data demonstrates that there is a direct correspondence between the frequency shift induced by the tip and the unperturbed electric field profile of the mode, accordingly to the findings in Refs. 15 and 16. More relevant, for the topic addressed here is the experimental observation that the spectral shift maps are also independent on the polarization configuration in the detection, including the absolute value of the mode shift and therefore we can conclude that the mode M2 is a single nondegenerate mode. The tip-induced spectral shift map gives a direct and high fidelity experimental imaging of the electromagnetic local density of states but, at least for nondegenerate modes, it does not provide selective information on the different electric field components.

Figure 3 shows, in the last column, the spatial distribution of the PL signal associated to mode M2 for three different polarization configurations ($\theta=0^\circ, 90^\circ, 45^\circ$) compared with the calculated intensity of the electric field components at different distances d from the membrane surface (first four

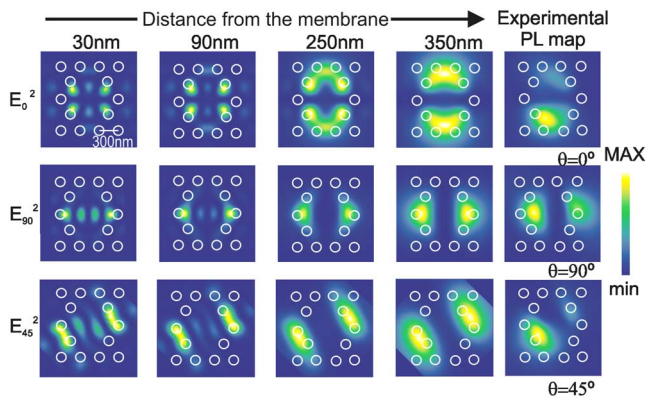


FIG. 3. (Color online) The first four columns report the calculated electric field components, associated to the cavity mode M2, as calculated at different height d from the membrane surface; in particular $d=30, 90, 250$, and 350 nm from the first to the fourth column. These data are compared with the experimental PL near-field maps, which are reported in the fifth and last column. The three rows correspond to different polarization configurations ($\theta=0^\circ, 45^\circ, 90^\circ$), as reported in the figure.

columns). The most strikingly aspect of the experimental data is that the PL intensity maps rotate when varying the polarization configuration. This clearly indicates that there is a direct link between the far-field control of the polarization and the near-field PL intensity maps and we interpret the polarization-sensitive PL maps as the near field maps of the corresponding electric field components. However, in order to reproduce the experimental PL maps, it is necessary to know the transfer function of the SNOM tip.²⁴ To simplify this problem it is commonly assumed that the near-field PL map measured by uncoated tips can be retraced by calculating the theoretical map at an effective distance d from the sample surface.^{24–26} The value of d does not represent the real height of the tip but it is an effective free parameter that deals with the fact that the collected signal is related to the electric field intensity distribution averaged over the normal axis of the sample weighted by the tip geometry. Therefore, the SNOM PL intensity map differs from the electric field intensity distribution in the sample surface.²⁵ The value of d would depend on both the mode propagation pattern and the tip geometry. The comparison between experimental and simulated PL maps clearly shows that all three experimental maps are well reproduced by the calculated intensity associated to electric field components for a distance d of 350 nm. It is also worth stressing that our findings (where the only fitting parameter is the distance d for all the three experimental maps) is an important validation test of the empirical procedure of using an effective distance d from the sample surface, when reproducing the PL experimental maps.

In conclusion, we demonstrate that it is possible to obtain polarization sensitive maps of PC cavity modes. In addition, the simultaneous analysis of different PL maps with the polarization control allowed us to obtain important insights on SNOM detection mechanisms.

Financial support is acknowledged from the Swiss National Science Foundation (Professeur boursier program). We

acknowledge Carmine Mastrandrea for helping in performing the micro-PL experiments.

- ¹Y. Akahane, T. Asano, B.-S. Song, and S. Noda, *Nature (London)* **425**, 944 (2003).
- ²S. Noda, M. Fujita, and T. Asano, *Nat. Photonics* **1**, 449 (2007).
- ³S. Strauf, K. Hennessy, M. T. Rakher, Y.-S. Choi, A. Badolato, L. C. Andreani, P. M. Petroff, E. L. Hu, and D. Bouwmeester, *Phys. Rev. Lett.* **96**, 127404 (2006).
- ⁴F. McNeillie, E. Riis, J. Broeng, J. Folkenberg, A. Petersson, H. Simonsen, and C. Jacobsen, *Opt. Express* **12**, 3981 (2004).
- ⁵K. Hennessy, C. Hogerle, E. Hu, A. Badolato, and A. Imamoglu, *Appl. Phys. Lett.* **89**, 041118 (2006).
- ⁶K. Hennessy, A. Badolato, M. Winger, D. Gerace, M. Atatüre, S. Gulde, S. Fält, E. L. Hu, and A. Imamoglu, *Nature (London)* **445**, 896 (2007).
- ⁷W.-H. Chang, W.-Y. Chen, H.-S. Chang, T.-P. Hsieh, J.-I. Chyi, and T.-M. Hsu, *Phys. Rev. Lett.* **96**, 117401 (2006).
- ⁸N. Louvion, D. Gérard, J. Mouette, F. de Fornel, C. Seassal, X. Letartre, A. Rahmani, and S. Callard, *Phys. Rev. Lett.* **94**, 113907 (2005).
- ⁹S. I. Bozhevolnyi, V. S. Volkov, J. Arentoft, A. Boltasseva, T. Sondergaard, and M. Kristensen, *Opt. Commun.* **212**, 51 (2002).
- ¹⁰P. Kramper, M. Kafesaki, C. M. Soukoulis, A. Birner, F. Müller, U. Gösele, R. B. Wehrspohn, J. Mlynek, and V. Sandoghdar, *Opt. Lett.* **29**, 174 (2004).
- ¹¹H. Gersen, T. J. Karle, R. J. P. Engelen, W. Bogaerts, J. P. Korterik, N. F. van Hulst, T. F. Krauss, and L. Kuipers, *Phys. Rev. Lett.* **94**, 073903 (2005).
- ¹²A. F. Koenderink, R. Wüest, B. C. Buchler, S. Richter, P. Strasser, M. Kafesaki, A. Rogache, R. B. Wehrspohn, C. M. Soukoulis, D. Ernig, F. Robin, H. Jäckel, and V. Sandoghdar, *Photonics Nanostruct. Fundam. Appl.* **3**, 63 (2005).
- ¹³K. Okamoto, M. Loncar, T. Yoshie, A. Scherer, Y. Qiu, and P. Gogna, *Appl. Phys. Lett.* **82**, 1676 (2003).
- ¹⁴F. Intonti, S. Vignolini, F. Riboli, A. Vinattieri, D. S. Wiersma, M. Colocci, M. Gurioli, L. Balet, C. Monat, L. H. Li, N. Le Thomas, R. Houdre, A. Fiore, M. Francardi, A. Gerardino, F. Roemer, and B. Witzigmann, *Physica E (Amsterdam)* **40**, 1965 (2008).
- ¹⁵A. F. Koenderink, M. Kafesaki, B. C. Buchler, and V. Sandoghdar, *Phys. Rev. Lett.* **95**, 153904 (2005).
- ¹⁶F. Intonti, S. Vignolini, F. Riboli, A. Vinattieri, D. S. Wiersma, M. Colocci, L. Balet, C. Monat, C. Zinoni, L. H. Li, R. Houdré, M. Francardi, A. Gerardino, A. Fiore, and M. Gurioli, *Phys. Rev. B* **78**, 041401(R) (2008).
- ¹⁷S. Mujumdar, A. F. Koenderink, T. Süner, B. C. Buchler, M. Kamp, A. Forchel, and V. Sandoghdar, *Opt. Express* **15**, 17214 (2007).
- ¹⁸L. Lalouat, B. Cluzel, P. Velha, E. Picard, D. Peyrade, J. P. Hugonin, P. Lalanne, E. Hadji, and F. de Fornel, *Phys. Rev. B* **76**, 041102(R) (2007).
- ¹⁹S. Vignolini, F. Intonti, L. Balet, M. Zani, F. Riboli, A. Vinattieri, D. S. Wiersma, M. Colocci, C. Monat, C. Zinoni, L. H. Li, M. Francardi, A. Gerardino, A. Fiore, and M. Gurioli, *Appl. Phys. Lett.* **93**, 023124 (2008).
- ²⁰M. Burreli, R. J. P. Engelen, A. Opheij, D. van Oosten, D. Mori, T. Baba, and L. Kuipers, *Phys. Rev. Lett.* **102**, 033902 (2009).
- ²¹R. Dandliker, P. Tortora, L. Vaccaro, and A. Nesci, *J. Opt., Pure Appl. Opt.* **6**, S18 (2004).
- ²²M. Francardi, L. Balet, A. Gerardino, C. Monat, C. Zinoni, L. H. Li, B. Alloing, N. Le Thomas, R. Houdré, and A. Fiore, *Phys. Status Solidi C* **3**, 3693 (2006).
- ²³R. Stöckle, C. Fokas, V. Deckert, R. Zenobi, B. Sick, B. Hecht, and U. P. Wild, *Appl. Phys. Lett.* **75**, 160 (1999).
- ²⁴J. A. Porto, R. Carminati, and J.-J. Greffet, *J. Appl. Phys.* **88**, 4845 (2000).
- ²⁵Y. De Wilde, F. Formanek, R. Carminati, B. Gralak, P.-A. Lemoine, K. Joulain, J.-P. Mulet, Y. Chen, and J.-J. Greffet, *Nature (London)* **444**, 740 (2006).
- ²⁶S. Vignolini, F. Riboli, F. Intonti, M. Belotti, M. Gurioli, Y. Chen, M. Colocci, L. C. Andreani, and D. S. Wiersma, *Phys. Rev. E* **78**, 045603(R) (2008).